Ferromagnetism induced by oxygen and cerium vacancies above the percolation limit in CeO_2

2010 J. Phys.: Condens. Matter 22 216004

(http://iopscience.iop.org/0953-8984/22/21/216004)

J. Phys.: Condens. Matter **22** (2010) 216004 (8pp) doi:10.1088/0953-8984/22/21/216004

Ferromagnetism induced by oxygen and cerium vacancies above the percolation limit in CeO_2

V Fernandes[1], P Schio[2], A J A de Oliveira[2], W A Ortiz[2], P Fichtner[3], L Amaral[4], I L Graff[5,6], J Varalda[5], N Mattoso[5], W H Schreiner[5] and D H Mosca[5]

[1] PIPE, Universidade Federal do Paraná, 81531-990 Curitiba PR, Brazil
[2] Departamento de Física, Universidade Federal de São Carlos, 13565-905, São Carlos, SP, Brazil
[3] Escola de Engenharia, Universidade Federal do Rio Grande do Sul, 91501-970 Porto Alegre, Brazil
[4] Instituto de Física, Universidade Federal do Rio Grande do Sul, 91501-970 Porto Alegre, RS, Brazil
[5] Departamento de Física, Universidade Federal do Paraná, 81531-990 Curitiba, PR, Brazil

Received 17 December 2009, in final form 15 April 2010
Published 5 May 2010
Online at stacks.iop.org/JPhysCM/22/216004

Abstract

We studied the structural, chemical and magnetic properties of non-doped ceria (CeO_2) thin films electrodeposited on silicon substrates. Experimental results confirm that the observed room temperature ferromagnetism is driven by both cerium and oxygen vacancies. We investigated ceria films presenting vacancy concentrations well above the percolation limit. Irradiation experiments with neon ions were employed to generate highly oxygen defective $CeO_{2-\delta}$ structures. X-ray photoelectron spectroscopy and x-ray absorption near-edge structure spectroscopy were used to estimate the concentration of Ce^{3+} sites in the films, which can reach up to 50% of Ce^{3+} replacing Ce^{4+}, compared to a stoichiometric CeO_2 structure. Despite the increment of structural disorder, we observe that the saturation magnetization continuously increases with Ce^{3+} concentration. Our experiments demonstrate that the ferromagnetism observed in ceria thin films, highly disordered and oxygen-deficient, preserving the fluorite-type structure only in a nanometer scale, remains intrinsically stable at room temperature.

(Some figures in this article are in colour only in the electronic version)

1. Introduction

Pure stoichiometric ceria (CeO_2) is diamagnetic, having a calcium fluoride structure over the whole temperature range up to melting point. In bulk, non-stoichiometric $CeO_{2-\delta}$ is a paramagnetic material with some Ce^{4+} ions replaced by Ce^{3+} ions. In this case, charge is balanced by some of the Ce^{3+} going to interstitial sites and mainly by formation of oxygen vacancies [1]. The electrons left behind by released oxygen are localized on cerium ions [2, 3]. Ceria preserves a fluorite structure even under a strongly oxygen deficient condition [2, 4], it being generally agreed that the main charge-compensating defects in $CeO_{2-\delta}$ are oxygen vacancies, since only a small amount of cerium vacancies would be favored by thermodynamics.

Room temperature ferromagnetism has been observed in undoped ceria-based nanostructures as films [5], nanoparticles [6], nanobelts [7], and nanocubes [8]. The origin of this magnetism is still under debate [9], but recent experimental works and band structure calculations proposed that ferromagnetism observed in ceria and several other undoped oxides, e.g., HfO_2 [10, 11], In_2O_3 [12], ZnO [13, 14], MgO [15], SnO_2 [16], and CuO_2 [17, 18] is due to the existence of intrinsic point defects. Most of these works explore the magnetism with a minimum concentration of defects; i.e., in the diluted defects limit. The magnetic interaction distance is arbitrarily established within percolation analyses. According to Osorio-Guillén *et al* [11] the onset of collective magnetic effects is approximately 20% in a cation sublattice having face-centered cubic symmetry, as in ceria. The ferromagnetism above the percolation limit is not obvious due to the possibility of compensation effects coming from

[6] Present address: Universidade Tecnológica Federal do Paraná—UTFPR, Av. Sete de Setembro 3165, Curitiba, Brazil.

the antiferromagnetically interacting vacancies, as pointed out for HfO_2 in [11]. In particular, CeO_2 films grown by the electrodeposition technique match several optimal properties for the development of multifunctional spintronic and optoelectronic devices, namely: semiconducting behavior, transparency in the visible wavelength range; high saturation magnetization and, nearly temperature independent magnetic behavior close to room temperature.

In the present work we have studied the defect-related origin of the ferromagnetism in non-stoichiometric CeO_2 films grown on Si wafers by electrodeposition. In order to investigate the effects of the amount of vacancies above the percolation threshold concentration, CeO_2 thin films were prepared under different growth conditions as well as being submitted to Ne^+ irradiations. The effects of oxidation level on the magnetic response of as-deposited and neon-irradiated films were evaluated by superconducting quantum interference device (SQUID) magnetization measurements. The crystalline structure of the films was monitored by using transmission electron microscopy.

2. Experiment

The CeO_2 films used in the present experiment were cathodically electrodeposited at room temperature using a stationary three-electrode cell with a galvanostat/potentiostat (EG&G model 273A). The working electrodes were single-side polished rectangular p-type Si(001) wafers with a resistivity of 10 Ω cm at room temperature. Hydrogen-terminated Si surfaces were obtained by removal of the native oxide via chemical HF-etching prior to electrochemical experiments. Gallium–aluminum alloying was used on the rear of the Si wafers to form a good ohmic contact. A standard saturated Ag/AgCl electrode was used as the reference electrode, while a platinum disk was used as the counter-electrode. Ceria films were deposited from bi-distilled aqueous solutions containing 800 μmol l^{-1} of $CeCl_3{\cdot}7H_2O$ with and without the addition of 20 mmol l^{-1} of hydrogen peroxide (H_2O_2) at cathodic potentials of −1.0 and −1.2 V, respectively, versus a Ag/AgCl reference electrode. Whereas the pH value remains 5.6 in the absence of additive, the addition of H_2O_2 leads to depositions with pH values varying from 4.0 to 3.5. Deposits with a small oxygen deficiency are attained from solutions containing H_2O_2 additive. The electrochemical experiments were performed in a dark chamber under controlled illumination of the electrolyte/Si interface through the solution using a halogen lamp with an infrared filter, providing a fairly uniform beam of visible light with an emission spectrum mainly distributed between 400 and 700 nm. The films used in this work are homogeneous, adherent and translucent, having thicknesses of about 20 nm, according to transmission electron microscopy. A detailed description of the electrochemical experiments and growth conditions is published elsewhere [19].

The crystalline structure of the films was investigated by transmission electron microscopy (TEM) through bright-field imaging and selected-area electron diffraction (SAED) analyses using a Jeol 1200 EX II microscope operating at 120 kV. To examine the chemical composition and stoichiometry of the films, x-ray photoelectron spectroscopy (XPS) analyses were performed using a VG ESCA3000 spectrometer equipped with a conventional Mg x-ray source and a hemispherical energy analyzer with an overall resolution of 0.8 eV at a 45° emission angle. A complementary characterization of the stoichiometry was carried out by x-ray absorption near-edge structure (XANES) spectroscopy, performed in fluorescence mode, using the D04B-XAFS1 beamline of the LNLS Synchrotron at Campinas, Brazil.

In order to generate vacancies in the as-deposited films, Ne^+ irradiation was performed at room temperature and pressure of 2×10^{-7} mbar using a beam current density around 0.5 μA cm^{-2}. The irradiation was performed with energies ranging from 30 to 350 keV. Ion-energy loss profiles calculated with the SRIM code [20] show that nuclear stopping power is more relevant for 30 keV than 350 keV; i.e., the electronic stopping power is stronger for higher energies. For all the ion energies used in this study, the ions traverse the whole film thickness (∼20 nm), going on to stop in the Si substrate. The effects of Ne^+ irradiation on the magnetism of films with surface areas ranging in between 0.09 and 0.12 cm^2 were studied by magnetization measurements at 298 K using a Quantum Design MPMS-5S SQUID magnetometer with an applied magnetic field in the film plane.

3. Results

To address the effects of the vacancies on the magnetic behavior of the films several approaches were used. As previously reported [5, 19], the oxygen deficiency in the deposited films can be changed during growth by adding hydrogen peroxide to the electrochemical solution. In this case, several ionic species can be formed and cerium hydroxides precipitation occurs in the solution. Nevertheless, the Ce^{3+} concentration in the films deposited with and without addition of hydrogen peroxide ranges between 3.3 and 20%. Then, ion irradiation, which is known to be one of the most efficient methods to induce defects in solid materials, was used to reach higher Ce^{3+} concentrations.

The hysteresis magnetic loops shown in figure 1 were measured for an as-prepared film using the hydrogen peroxide additive and also after sequential irradiation with Ne^+ ions at energies of 200 and 90 keV with a total fluence of 2×10^{16} ions cm^{-2}. The aim of these irradiations at two ion energies was to attain a more or less uniform damage profile in the film, as calculated by SRIM. Interestingly, the irradiated film presents a saturation magnetization of 220 emu cm^{-3}, a value 38% higher than the as-deposited one[7]. The inset of figure 1 shows the inner part of the loops revealing coercive

[7] The sample prepared with H_2O_2 additive called as-deposited in this work is used as a reference for magnetic data comparisons. This sample is the same Sample B presented in [5]. However, the hysteresis loop corresponds to another slice of Sample B [5]. The reader could also note the difference in the saturation magnetization values found in these two works. This discrepancy is justified by an overestimated thickness obtained by the faradaic method in [5]. Recent high-resolution cross-sectional transmission electron microscopy analysis of the samples revealed average thicknesses of 20 nm instead of the 30 nm cited in [5].

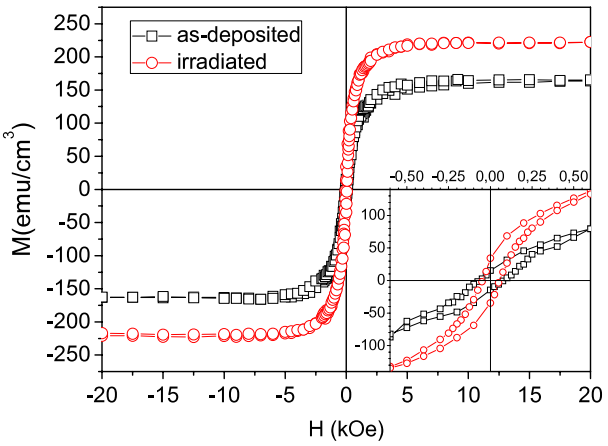

Figure 1. Comparison between hysteresis magnetic loops of the film immediately after deposition from the solution containing the H_2O_2 additive and after sequential irradiation with Ne^+ ions at energies of 200 and 90 keV with 2×10^{16} ions cm^{-2}. The inset shows the inner part of the hysteresis cycles.

fields between 50 and 70 Oe. Remanent magnetization increases from 9 to 15% as a result of the irradiation.

TEM experiments were used to follow the structural disorder induced by ion irradiation in the films. According to the SAED patterns shown in figure 2(a), the as-deposited film has a predominant nanocrystalline structure. The interplanar spacings determined from the diffraction ring diameters are clearly associated with the Bragg reflections of a cubic fluorite-type CeO_2 structure. The space group corresponds to $Fm3m$ and the lattice parameter is $a = 0.541$ nm (ICDS database no. 28785). The SAED pattern shown in figure 2(b) corresponds to the same film after sequential irradiation with Ne^+ ions at energies of 200 and 90 keV with a fluence of 10^{16} ions cm^{-2}. Clearly, the remaining diffraction rings become wider and diffuse, indicating a degradation of the crystalline quality. The corresponding intensity profiles of the SAED patterns are shown in figures 2(c) and (d). The continuous background is significantly enhanced after irradiation as a result of the structural disorder, showing that such a film possesses an important amorphous fraction.

X-ray photoelectron spectroscopy (XPS) measurements were performed by collecting the spectra immediately after turning on the x-ray source to avoid any induced artifacts associated with the reduction of ceria by the heating from the x-ray beam [14]. XPS analyses indicate that the deposits exhibit an elemental composition consisting of Ce and O with a residual layer consisting of N and C adsorbates. Within the instrumental sensitivity, neither contamination (from the precursors) nor intermediate compounds have been detected.

XPS spectra of Ce 3d core-level regions for the as-deposited film are shown in figure 3(a). The energy position of the Si 2p core-level was used to correct the energy shifts due to the charging effects. There are ten deconvoluted-Gaussian peak assignments in the spectra: peaks labeled as U, U″, U‴ (V, V″, V‴) refer to $3d_{3/2}$ ($3d_{5/2}$) and are characteristic of Ce^{4+} 3d final states; while U_0, U′ (V_0, V′) refer to $3d_{3/2}$ ($3d_{5/2}$) for Ce^{3+} 3d final states [21]. The peaks labeled V and V″ have been assigned to a mixing of Ce $3d^9$ $4f^2$ O $2p^4$ and Ce $3d^9$ $4f^1$ O $2p^5$ of Ce^{4+} final states, and the peak denoted by

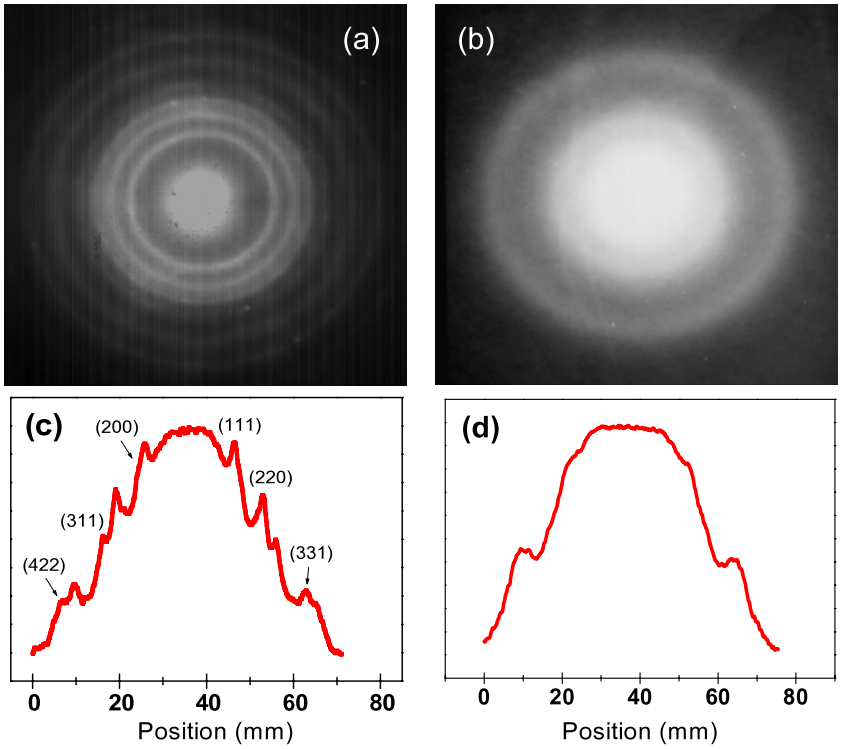

Figure 2. SAED patterns corresponding to films (a) as-deposited from a solution containing H_2O_2 additive (the inset of figure 1(b) in [5]) and (b) after sequential implantation with Ne^+ ions at 200 and 90 keV. The corresponding SAED intensity profiles are shown in (c) and (d). Diffraction rings associated with fluorite structure of CeO_2 are indexed.

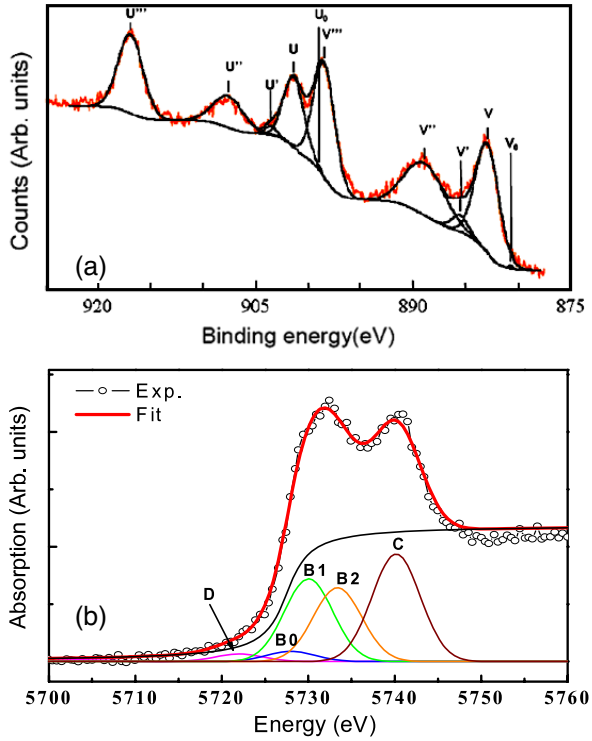

Figure 3. (a) Ce 3d core-level XPS spectra (figure 2(b) in [5]) and (b) Ce L_{III} XANES spectra of film as-deposited from solutions containing hydrogen peroxide additive.

V‴ corresponds to the Ce $3d^9$ $4f^0$ O $2p^6$ of the Ce^{4+} final state. On the other hand, lines V_0 and V′ are assigned to Ce $3d^9$ $4f^2$ O 2p5 and Ce $3d^9$ $4f^1$ O $2p^6$ of the Ce^{3+} final state. The same assignment can be applied to the U structures, which correspond to the Ce $3d_{3/2}$ levels.

The relative weight between the fitted peak areas of Ce^{4+} and Ce^{3+} components for ceria can be used to estimate the contributions of Ce^{4+} and Ce^{3+} valence states. The presence of Ce^{3+} implies a $CeO_{2-\delta}$ defect structure, i.e., reflects the oxygen vacancies (V_O) concentration [22]. The Ce^{3+} concentration in the films was determined as follows:

$$[Ce^{3+}] = \frac{A_{V0} + A_{V'} + A_{U0} + A_{U'}}{A_{V0}+A_{V'}+A_{U0}+A_{U'}+A_V+A_{V''}+A_{V'''}+A_U+A_{U''}+A_{U'''}}, \quad (1)$$

where $A_V(A_U)$ are the areas of each spectral peak. Ce^{3+} concentration is estimate as 3.3% for the film deposited from the solution with H_2O_2 additive and 18.7% after sequential Ne-irradiation with energies of 200 and 90 keV. It is interesting to note the saturation magnetization M_S found for the irradiated film (220 emu cm^{-3} is found with Ce^{3+} concentration of 18.7%) are in agreement with that observed for a film deposited without H_2O_2 additive (244 emu cm^{-3} is found with Ce^{3+} concentration of 22.7%). The individual contributions of the Ce^{3+} and Ce^{4+} species to the whole Ce 3d spectrum were determined by quantitative analysis, involving ten peaks with correlations and restrictions to reduce the parameters, such as the relations of intensities for doublets due to orbit–spin coupling and separation in binding energies. For convenience, we have assumed that cerium vacancies (V_{Ce}) are low and do not affect the determination of Ce^{3+} species by XPS, although V_{Ce} is plausible in the films after irradiation. Our results are summarized in table 1.

Table 1. Ce^{3+} concentration as determined by XPS analyses and saturation magnetization M_S determined by SQUID magnetometry for several samples: as-deposited (as-dep) with (w/) and without (w/o) H_2O_2 additive, film prepared with H_2O_2 additive and aged in the atmospheric conditions by 24 months, and Ne-irradiated films.

Samples	Energy (keV)	Fluence (ions cm^{-2})	Ce^{3+} (%)	M_S (emu cm^{-3})
Aged in atmosphere	—	—	∼0.0	10
As-dep w/H_2O_2	—	—	3.3	160
Irradiated	90/200	2×10^{16}	18.7	220
As-dep w/o H_2O_2	—	—	22.7	244
Irradiated	30	2×10^{16}	47.2	372
		2×10^{14}	44.6	312
	350	2×10^{16}	41.0	335
		2×10^{14}	23.7	136

It is worth pointing out that XPS technique is an excellent surface probe, being sensitive to a layer that is frequently 5–20 nm depending upon the kinetic energy of electrons and the materials. For instance, the escape depth of 3d photoelectrons is about 6 nm with an inelastic mean free path of ∼1.2 nm. Such small escape distances require an ultra-high vacuum (UHV) environment ($<10^{-9}$ Torr) for the analysis chamber, which in turn may cause the reduction of CeO_2 films near the surface after a prolonged exposure to the x-ray beam. In fact, previous studies have reported that ceria loses surface oxygen when exposed to low oxygen partial pressure and when irradiated by x-rays in the XPS chamber [23, 24]. Combination of XPS and XANES has already been employed to study the reduction dynamics and oxygen diffusion of ceria nanoparticles [25]. Both the diffuse depth profile of the Ce^{3+} concentration as well as the unintended surface reduction of ceria induced by x-ray exposure have been reported.

To check this point and to get an estimate of Ce^{3+} concentration in the volume of the film, we performed XANES measurements, the results of which are shown in figure 3(b). A peak fitting method was applied to estimate Ce^{3+} concentrations from the Ce L_{III} XANES spectra. Peaks were fitted with Gaussian functions and an arctan function was subtracted to simulate the edge jump in the spectra [26, 27]. According to previous studies, the Ce L_{III} XANES spectrum of CeO_2 results from the configuration interaction due to mixing of Ce 4f and O 2p valence orbitals associated with the crystal-field splitting of the Ce 5d final state [28, 29]. The peak assigned as C in figure 3(b) is a Ce^{4+} peak and corresponds to a final state of $2p4f^05d^1$. Spectral components B1 and B2 also comprise a Ce^{4+} peak with a final state of $2p4f^15d^1v$, which denotes that in addition to an electron excited from the Ce 2p shell to the 5d shell, another electron is also excited from the valence band (O 2p shell) to the Ce 4f shell, leaving a hole (represented by v above) in the valence band. At the pre-edge region there is peak denoted by D arising from a dipole-forbidden transition due to transitions at the bottom

of the conduction band [29]. In our case, the as-deposited CeO_2 sample contains a small quantity of Ce^{3+}, as shown by XPS data in figure 3(a). The XANES spectrum of a Ce^{3+} compound, such as for instance $Ce(OH)_3$, is characterized by a single white line at the edge [30]. The peak is located at smaller energies than B1, about 2.0 eV apart, and we designated it as B0. Keeping this in mind one may use the spectral weight of peak B0, namely I_{B0}, as an estimate of Ce^{3+} concentration as follows:

$$[Ce^{3+}] = \frac{I_{B0}}{I_{B0} + I_{B1} + I_{B2} + I_C}. \quad (2)$$

XANES analyses using Athena software [31] leads to the Ce^{3+} concentration for the as-deposited film as being 3.7%, which is in good agreement with the XPS result (3.3%). Then, in our case a surface reduction of ceria by XPS is not confirmed by XANES. Since the CeO_2 XANES analyses is complex, we have used the more accessible and well-established XPS technique for further evaluations of Ce^{3+} concentration in our samples.

To study the magnetization dependence on the number of cerium and oxygen vacancies, a set of films was deposited from solutions without H_2O_2 additive but subsequently irradiated with 30 and 350 keV Ne^+ ions at fluences of 2×10^{14} and 2×10^{16} ion cm^{-2} with targets kept at room temperature. Slices of the same as-deposited film were used in the comparative analyses. SRIM simulations show that for CeO_2 films irradiated with 30 keV Ne^+ ions, the energy loss over the film thickness corresponds to 43% (57%) of electronic (nuclear) loss. In the case of CeO_2 films irradiated with 350 keV Ne^+ ions, the energy loss corresponds to 87% (13%) electronic (nuclear). SRIM simulations also give an estimated proportion of about 1:10 between oxygen vacancies (V_O) and cerium vacancies (V_{Ce}) for both ion energies.

XPS spectra of Ne-irradiated films exhibit spectral components associated with partially reduced ceria. For example, a decrease of the intensity of the U‴ peak with increasing reduction of the ceria is observed. The decrease is far from being linear with the Ce^{3+} concentration as determined by equation (1), and some misfitting occurs around the position of the U‴ peak associated with Ce^{4+} when the percentage of Ce^{3+} increases. A nonlinear decrease of the U‴ Ce^{4+} peak, together with more intense U_o/V_o doublet peaks, is observed at a high level of reduction, as already reported by Holgado *et al* [32]. The intensities of both U_o/V_o and U′/V′ doublets associated with primary photoemission from the Ce^{3+} relative to the intensities of the photoemission peaks from Ce^{4+} increase up to 48.6%, as confirmed in table 1. It is important to emphasize that even if a preferential release of oxygen at surface is induced by Ne ion irradiation, leading to a high level reduction close to the surface of the films, the spectral shape characteristic of a Ce_2O_3—like reference was not observed by XPS [32, 33].

Magnetic measurements were performed for all the irradiated films. The magnetization of the as-deposited film with the lowest concentration of oxygen vacancies (prepared with additive) will be used as a reference for the saturation magnetization values. Figure 4 exhibits hysteresis magnetic loops for the as-deposited film and irradiated films. In

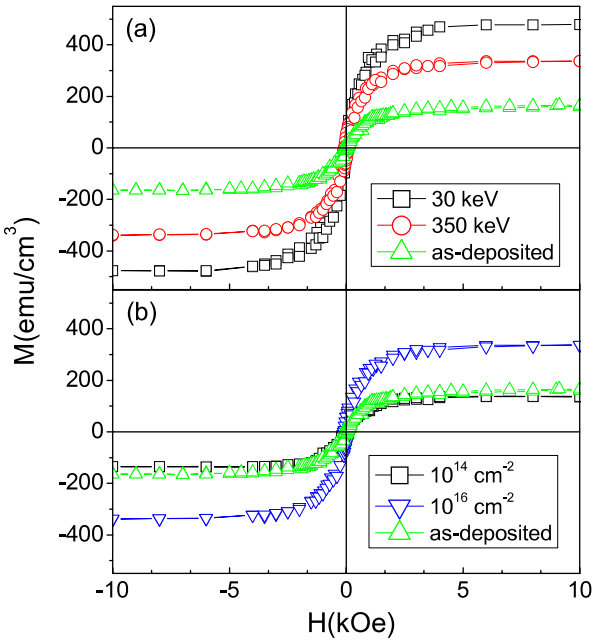

Figure 4. Comparison between hysteresis magnetic loops of the film immediately after deposition from a solution containing H_2O_2 additive and films (a) after irradiation with 30 and 350 keV Ne^+ ions at 2×10^{16} ions cm^{-2}, and (b) after irradiation with 350 keV Ne^+ ions at 2×10^{14} and 2×10^{16} ions cm^{-2}.

figure 4(a), the M_S value is higher for the film irradiated with 30 keV Ne^+ ions at a fluence of 2×10^{16} ions cm^{-2} than for the film irradiated with 350 keV Ne^+ ions at the same fluence, and both irradiated films exhibit M_S greater than the as-deposited one. We recall that the as-deposited film presents a lower V_O and a still lower V_{Ce}. Furthermore, SRIM simulations indicate that Ne-irradiation generates more V_{Ce} than V_O. It is worth noting that SRIM simulations give results from a ballistic scenario; i.e., thermodynamic effects such as dynamic annealing during irradiation are not taken into account. We are aware that a significant amount of the ballistic-produced defects will recombine, the final amount of defects being smaller than the ones given by SRIM.

The magnetization dependence on the ion fluence, for films irradiated with 350 keV Ne^+ ions is shown in figure 4(b), again compared to as-deposited film prepared with the additive. M_S value is approximately the same as the as-deposited film when the fluence is 2×10^{14} ions cm^{-2}. Increasing the fluence to 2×10^{16} ions cm^{-2} the M_S value increases. In this case, the irradiated film is rather disordered exhibiting an equivalent probability of ionic sites with Ce^{3+} and Ce^{4+} valence states. Table 1 summarizes our results of saturation magnetization (M_S) and Ce^{3+} concentration. Our films having a Ce^{3+} concentration varying from nominal 0 to 47.2% exhibit soft-magnetic behavior with saturation magnetization values ranging between 10 and 372 emu cm^{-3}, remanences between 6 and 18% and coercive fields smaller than 100 Oe. Our magnetic data indicate a rather robust ferromagnetic behavior at room temperature even with the structural disorder induced by ion irradiation. According to table 1, a trend is observed in which the saturation magnetization increases with Ce^{3+} concentration.

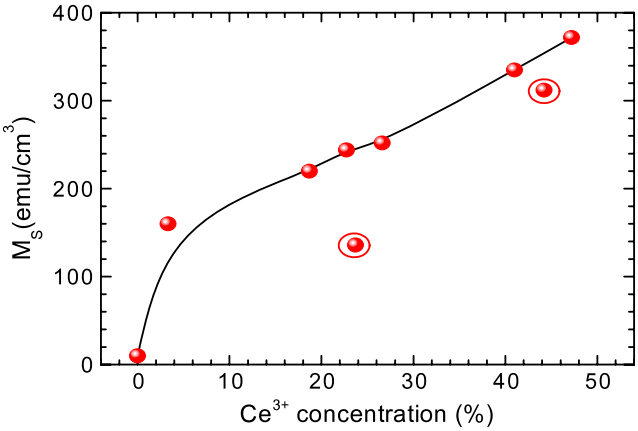

Figure 5. Saturation magnetization as a function of the Ce^{3+} concentration. The two circled points correspond to Ne-irradiation with fluences of 2×10^{14} ions cm^{-2}. The solid line is just to guide the eyes.

4. Discussion

Pristine CeO_2 films electrodeposited from solutions in the presence of H_2O_2 additive exhibit low V_O concentration (about 1.7% by assuming two Ce^{3+} sites per V_O), whereas films deposited without the additive exhibit higher V_O concentration. The presence of V_{Ce} is plausible in both films. However, the large energy necessary to remove Ce^{4+} ions having eightfold-coordination makes the expectation for V_{Ce} formation very low under thermodynamic equilibrium. The observed saturation magnetization in films exposed to the air for several months is non-negligible, being mainly associated with the presence of V_{Ce} [5] in as-deposited films with Ce^{3+} concentration lower than our XPS sensitivity. The non-negligible amount of V_{Ce} comes from the fact that electrodeposition is a non-equilibrium technique. A further intentional increase of V_{Ce} with respect to V_O can be achieved through ion irradiation and it could emphasize the dependence of the ferromagnetic behavior in ceria films on V_{Ce}. The smaller M_S values at low V_O concentration (10 emu cm^{-3}) could be attributed to experimental artifacts, such as contamination and impurities in the handling of samples as well as malpractice in the measurements procedures, which produces magnetization values as high as 30–50 emu cm^{-3} [34–37]. However, we found M_S values as high as 370 emu cm^{-3}. Also, a direct correlation between M_S and Ce^{3+} concentration evidenced in figure 5 excludes erratic results associated with spurious sources of magnetism.

SRIM simulations indicate that irradiations with Ne ions could increase V_{Ce} with respect to V_O, even if V_O still remains the most important native defect over a wide range of conditions. Undoubtedly, vacancies and oxygen interstitials, as well as cerium antisites, are also generated by ion irradiation. Previous work reported by Ohno *et al* [33] on the effects of swift heavy ion irradiation in ceria (films and bulk) have shown a decrease in the coordination number of O atoms around Ce, whereas the valence state of Ce atoms is partly changed from +4 to +3 by the irradiation. To explain such effects the contribution of the electronic excitation induced by the incident ions has to be considered. In recent experiments, Ti^{3+} ion complexes in undoped TiO_2 films associated with oxygen vacancies generated by ion implantation were related to the observation of ferromagnetism at room temperature [38]. These results are in agreement with our present experiments and corroborate our conclusions.

Ne-irradiated films exhibit a large deviation in their stoichiometry, which is associated with oxygen deficiency followed by XPS analyses. Concomitantly, irradiated films present a significant amorphous fraction. From SRIM simulations the vacancy (both V_O and V_{Ce}) concentrations are increased by ion irradiation. More vacancies are expected for films irradiated with 30 keV Ne^+ ions than those irradiated with 350 keV, since vacancies are mainly generated by atomic collisions, that is, the number of vacancies will be greater for small irradiation energies, which present high nuclear energy loss. The number of vacancies and ion-induced damage is also expected to increase with the fluence.

XPS analyses indicate high reduction levels of Ce^{3+} in our irradiated ceria films. Low reduction levels of Ce^{3+} are associated with V_O, which in general are clustered as pairs. These clusters are precursors, after a deeper reduction [32], of defect strings mainly ordered along the ⟨111⟩ crystallographic directions of the parent fluorite lattice. Vacancies (both V_O and V_{Ce}) and disorder are expected to increase with ion fluence. A plot of M_S versus Ce^{3+} concentration for the several kinds of films studied is shown figure 5. Also included was the magnetic data used in [5]. In particular, there is a residual magnetization for a thin film stored for 24 months under atmospheric conditions, which becomes almost stoichiometric due to air-oxidation.

One important issue experimentally revealed is that films either before or after irradiation presents low remanence values. Development of a multiaxial anisotropy, state of stress, and demagnetizing effects associated with the formation of domain walls at grain boundaries are some possible reasons, but this is still not clear. To shed some light on this issue visualization methods of the magnetic domains are necessary.

A rapid increase in M_S for Ce^{3+} concentration below 20% is observed in figure 5. It is followed by a nearly linear increase of M_S for Ce^{3+} concentration up to 47.2%. Since the V_{Ce} number is not expected to change significantly at room temperature due to the aging effect, the rapid increase in M_S suggests that the presence of both V_O and V_{Ce} are important in stabilizing the ferromagnetism. On other hand, the nearly linear increase of M_S at high Ce^{3+} concentration suggests that the interaction between vacancies does not inhibit the ferromagnetism. The possibility of compensation effects coming from the antiferromagnetically interacting vacancies, as predicted by Osorio-Guillén *et al* [11] in undoped HfO_2, are not consistent with our findings. Our present results are also in contrast with statements given by Liu *et al* [39] that M_S is independent of V_O concentration in undoped CeO_2 prepared as nanopowders. These authors claim that post-annealing, conducted either in air or in a very reducing environment, lead to powdered samples without ferromagnetic signals. We believe that this controversial result

is partly due to the crystalline structure of the synthesized precipitates, which before and after annealing probably had negligible amounts of V_{Ce}. On the other hand, the defect-induced magnetism depends on the V_O location in the parent fluorite structure [9] and the vacancy probe technique used in [39] lacks the sensitivity to detect small changes in the surface stoichiometry. Shah *et al* [40] showed in a recent work that even Co-doped CeO_2 bulk samples exhibit room temperature ferromagnetism intimately linked with oxygen vacancies. Both experimental and first-principles calculations reinforce the crucial role of oxygen vacancies, suggesting that a ferromagnetic exchange mechanism involves a spin-polarized electron trapped at oxygen vacancy sites. Perhaps the relationship between the surface chemical states and magnetic properties pointed out by Li *et al* [41] in CeO_2 nanoparticles could explain the contradictory results described by Liu *et al* [39]. According to Li *et al* [41] the ferromagnetism does not relate to the surface oxygen vacancies, but to the mixed valent Ce^{3+}/Ce^{4+} pairs of the surface layer. Anyway, the saturation magnetization as a function of the number of mixed valent Ce^{3+}/Ce^{4+} pairs of CeO_2 nanoparticles shown in figure 4 of [41] are in good agreement with our present results.

5. Conclusion

The present experiments demonstrate that starting from pristine CeO_2 films with negligible oxygen deficiency it is possible to obtain a significant increase of the saturation magnetization by increasing the Ce^{3+} concentration. These experiments corroborate our previous band structure calculations in the diluted defects limit [5] and lead us to confirm a defect-induced origin for the ferromagnetism in non-doped ceria, even above the percolation limit of magnetically interacting vacancies. In addition, we demonstrate that the presence of a certain degree of disorder does not inhibit the ferromagnetism. Band structure calculations using density functional theory [5] can provide a possible explanation for the robustness of the ferromagnetic response. In these calculations it is found that spin-polarized charge density around vacancy sites leads to an electronic structure with an energy minimum for the global ferromagnetic state. Therefore, the observed magnetism in our films, consisting of CeO_2 nanograins, probably indicates that the persistent ferromagnetism is due to the fluorite-type structure, which is preserved at the nanoscale, even under strongly oxygen deficient conditions.

In conclusion, we report on the structural, chemical and magnetic properties in non-doped CeO_2 thin films electrodeposited on silicon substrates. The robust ferromagnetism observed in CeO_2 films is attracting a great deal of interest due to its potential for application in multifunctional devices. A wide bandgap magnetic oxide material with a high Curie temperature would be of tremendous interest to the emerging technology of spintronics. Furthermore, we believe that our findings on room temperature ferromagnetism in CeO_2 are important to the understanding of the novel magnetism currently observed in several other non-doped oxide materials.

Acknowledgments

We thank the Brazilian agencies CNPq, CAPES and FAPESP (Grant no. 2008/10276-5) for financial support. We also acknowledge technical support given by Centro de Microscopia Eletrônica at UFPR and the D04B-XAFS1 beamline staff of the LNLS as well as J J Klein for technical assistance with XPS measurements.

References

[1] Mogensen M, Sammes N M and Tompsett G A 2000 *Solid State Ion.* **129** 63
[2] Skorodumova N V, Simak S I, Lundqvist B L, Abrikosov I A and Johansson B 2002 *Phys. Rev. Lett.* **89** 166601
[3] Zhang C, Michaelides A, King D A and Jenkins S J 2009 *Phys. Rev.* B **79** 075433
[4] Steele B C H 2000 *Solid State Ion.* **129** 95
[5] Fernandes V, Mossanek R J O, Schio P, Klein J J, de Oliveira A J A, Ortiz W A, Mattoso N, Varalda J, Schreiner W H, Abbate M and Mosca D H 2009 *Phys. Rev.* B **80** 035202
[6] Sundaresan A, Bhargavi R, Rangarajan N, Siddesh U and Rao C N R 2006 *Phys. Rev.* B **74** 161306
[7] Li G R, Qu D L and Tong Y X 2008 *Electrochem. Commun.* **10** 80
[8] Ge M Y, Wang H, Liu E Z, Jiang J Z, Li Y K, Xu Z A and Li H Y 2008 *Appl. Phys. Lett.* **93** 062505
[9] Han X, Lee J and Yoo H I 2009 *Phys. Rev.* B **79** 100403
[10] Coey J M D, Venkatesan M, Stamenov P, Fitzgerald C B and Dorneles L S 2005 *Phys. Rev.* B **72** 024450
[11] Osorio-Guillén J, Lany S, Barabash S V and Zunger A 2007 *Phys. Rev.* B **75** 184421
[12] Hong N H, Sakai J, Poirot N and Brizé V 2006 *Phys. Rev.* B **73** 132404
[13] Wang Q, Sun Q, Chen G, Kawazoe Y and Jena P 2008 *Phys. Rev.* B **77** 205411
[14] Barnerjee S, Mandal M, Gayathri N and Sardar M 2007 *Appl. Phys. Lett.* **91** 182501
[15] Hu J, Zhang Z, Zhao M, Qin H and Jiang M 2008 *Appl. Phys. Lett.* **93** 192503
[16] Rahman G, Garcia-Suarez V M and Hong C 2008 *Phys. Rev.* B **78** 184404
[17] Soon A, Cui X Y, Delley B, Wei S H and Stampfl C 2009 *Phys. Rev.* B **79** 035205
[18] Chen C, He L, Lai L, Zhang H, Lu J, Guo L and Li Y 2009 *J. Phys.: Condens. Matter* **21** 145601
[19] Fernandes V, Klein J J, Schreiner W H, Mattoso N and Mosca D H 2009 *J. Electrochem. Soc.* **156** E199
[20] Biersack J P and Haggmark L G 1980 *Nucl. Instrum. Methods* **174** 257 SRIM code on the web: www.srim.org
[21] Burroughs P, Hamnett A, Orchard A F and Thornton G J 1976 *Chem. Soc. Dalton Trans.* **17** 1686
[22] Patsalas P, Logothetidis S, Sygellou L and Kennou S 2003 *Phys. Rev.* B **68** 035104
[23] Paparazzo E, Ingo G M and Zacchetti N 1991 *J. Vac. Sci. Technol.* A **9** 1416
[24] Rao M V R and Shripathi T J 1997 *Electron Spectrosc. Relat. Phenom.* **87** 121
[25] Zhang F, Wang P, Koberstein J, Khalid S and Chan S W 2004 *Surf. Sci.* **563** 74
[26] Nachimuthu P, Shih W C, Liu R S, Jang L Y and Chen J M 2000 *J. Solid State Chem.* **149** 408
[27] Shahin A M, Grandjean F, Long G J and Schuman T P 2005 *Chem. Mater.* **17** 315
[28] Bianconi A, Marcelli A, Dexpert H, Karnatak R, Kotani A, Jô T and Petiau J 1987 *Phys. Rev.* B **35** 806

[29] Soldatov A V, Ivanchenko T S, Della Longa S, Kotani A, Iwamoto Y and Bianconi A 1994 *Phys. Rev.* B **50** 5074
[30] El Fallah J, Boujana S, Dexpert H, Kiennemann A, Majerus J, Touret O, Villain F and Le Normand F 1994 *J. Phys. Chem.* **98** 5522
[31] Ravel B and Newville M 2005 *J. Synchrotron Radiat.* **12** 537
[32] Holgado J P, Alvarez R and Munuera G 2000 *Appl. Surf. Sci.* **161** 301
[33] Ohno H, Iwase A, Matsumura D, Nishihata Y, Mizuki J, Ishikawa N, Baba Y, Hirao N, Sonoda T and Kinoshita M 2008 *Nucl. Instrum. Methods Phys. Res.* B **266** 3013
[34] Grace P J, Venkatesan M, Alaria J, Coey J M D, Kopnov G and Naaman R 2009 *Adv. Mater.* **21** 71
[35] Garcia M A, Fernandez Pinel1 E, de la Venta J, Quesada A, Bouzas V, Fernández J F, Romero J J, Martín González M S and Costa-Krämer J L 2009 *J. Appl. Phys.* **105** 013925
[36] Golmar F, Mudarra Navarro A M, Rodríguez Torres C E, Sánchez F H, Saccone F D, dos Santos Claro P C, Benítez G A and Schilardi P L 2008 *Appl. Phys. Lett.* **92** 262503
[37] Abraham D W, Frank M M and Guha S 2005 *Appl. Phys. Lett.* **87** 252502
[38] Zhou S, Cizmar E, Potzger K, Krause M, Talut G, Helm M, Fassbender J, Zvyagin S A, Wosnitza J and Schmidt H 2009 *Phys. Rev.* B **79** 113201
[39] Liu Y, Lockman Z, Aziz A and MacManus-Driscoll J 2008 *J. Phys.: Condens. Matter* **20** 165201
[40] Shah L R, Ali B, Zhu H, Wang W G, Song Y Q, Zhang H W, Shah S I and Xiao J Q 2009 *J. Phys.: Condens. Matter* **21** 486004
[41] Li M, Ge S, Qiao W, Zhang L, Zuo Y and Yan S 2009 *Appl. Phys. Lett.* **94** 152511